OPTICAL KNIFE-EDGE DISPLACEMENT SENSOR MODELING

Ross Zameroski[1], Michael Gomez[2], and Tony Schmitz[1,2]
[1]Department of Mechanical, Aerospace, and Biomedical Engineering
University of Tennessee, Knoxville
Knoxville, TN 37996, USA
[2]Manufacturing Science Division
Oak Ridge National Laboratory
Oak Ridge, TN, 37830, USA

ABSTRACT
This paper describes an analytical model for the well-known optical knife-edge displacement sensor that predicts the relationship between the knife-edge displacement and photointerrupter output. The model includes: 1) the geometry of a rectangular knife-edge profile penetrating a circular laser beam perpendicular to the beam axis; and 2) the (assumed) Gaussian intensity profile for the beam cross-section. A comparison between the model predictions and measured photointerrupter for a linear range of knife-edge displacements is provided. It is shown that good agreement is obtained without model calibration.

KEYWORDS
Displacement, optical, knife-edge

INTRODUCTION
Optical beam profiling and dynamic displacement measurement are common applications of the knife-edge technique. In this approach, the knife-edge partially blocks the beam of interest and the unblocked portion is incident on a photodetector that generates an electrical signal proportional to intensity [1-17]. The photodetector voltage output varies from a maximum value (fully unblocked) to zero (fully blocked) as the knife-edge is displaced transversely across the beam's cross-section. The knife-edge position vs. photodetector voltage is nonlinear but may be linearized by selecting a region where is the beam is approximately 50% blocked. This is the typical approach so that the displacement may be calculated from voltage using only a calibration constant (e.g., µm/V).

The purpose of this paper is to consider both the geometry of a rectangular knife edge passing through a laser beam perpendicular to the beam axis and the (assumed) Gaussian beam profile to analytically predict the displacement-photodetector output relationship. This model may then be used to pre-select the linear range for the optical knife-edge displacement sensor because the linear range has design implications when integrating the sensor in an electromechanical system for measurement and/or control.

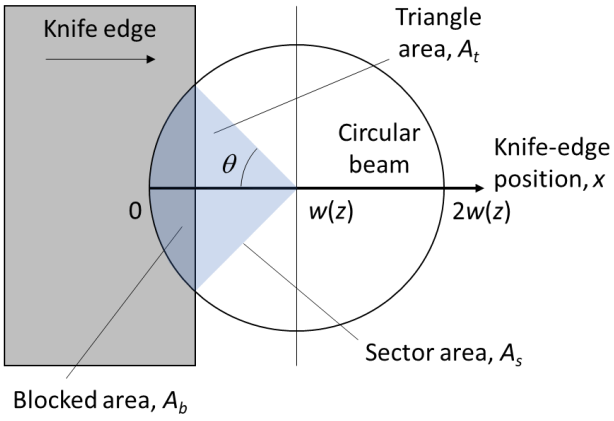

FIGURE 1. Blocked area geometry as the knife-edge covers the circular laser beam. The x = 0 knife-edge position represents fully unblocked and x = 2w(z) represents fully blocked.

OPTICAL KNIFE-EDGE DISPLACEMENT SENSOR MODELING
The model incorporates the basic geometry of the rectangular knife-edge penetrating a circular beam, while also considering the radially-

[2]Notice: This manuscript has been authored by UT-Battelle, LLC, under contract DE-AC05-00OR22725 with the US Department of Energy (DOE). The US government retains and the publisher, by accepting the article for publication, acknowledges that the US government retains a nonexclusive, paid-up, irrevocable, worldwide license to publish or reproduce the published form of this manuscript, or allow others to do so, for US government purposes. DOE will provide public access to these results of federally sponsored research in accordance with the DOE Public Access Plan (http://energy.gov/downloads/doe-public-access-plan).

symmetric Gaussian intensity distribution for the beam's cross-section. The model geometry is displayed in Fig. 1, where the knife-edge moves from left to right to sequentially block the laser beam. At any position, x, the blocked area, A_b, depends on x and the beam radius, $w(z)$. As shown in Fig. 2, the beam radius is a function of the location along the beam's propagation direction, z, and is minimum at the beam waist.

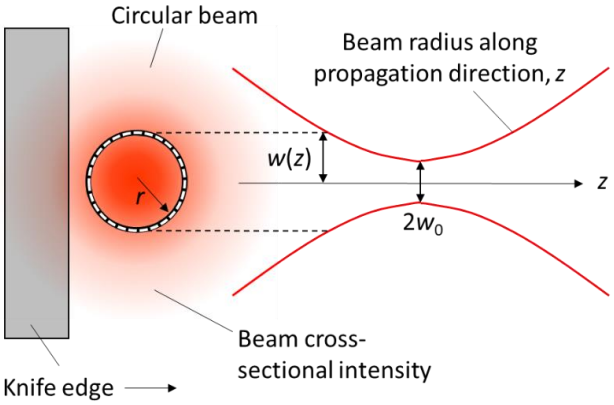

FIGURE 2. Beam intensity variation in the radial direction, r. The beam radius, w(z), is a function of the location along the beam propagation direction, z, and is minimum at the beam waist where the beam radius is w_0 and z = 0.

The blocked area can be calculated by recognizing that the shaded sector area, A_s, in Fig. 1 is composed of the blocked area (represented by the darker shading) and two right triangles. The sector area is:

$$A_s = w(z)^2\theta, \tag{2}$$

where the half-angle, θ, for the sector is:

$$\theta = \operatorname{acos}\left(\frac{w(z)-x}{w(z)}\right). \tag{3}$$

The area, A_t, for both the upper and lower right triangles in Fig. 1 (top panel) is:

$$A_t = \frac{1}{2}(w(z)-x)\sqrt{w(z)^2-(w(z)-x)^2}. \tag{4}$$

The blocked area is calculated using Eq. 5. The nonlinear variation in blocked area with knife-edge position is plotted in Fig. 3. The blocked area is normalized to the beam cross-sectional area, $A = \pi w(z)^2$, for generality.

$$A_b = A_s - 2A_t = w(z)^2\operatorname{acos}\left(\frac{w(z)-x}{w(z)}\right) - (w(z)-x)\sqrt{w(z)-(w(z)-x)^2} \tag{5}$$

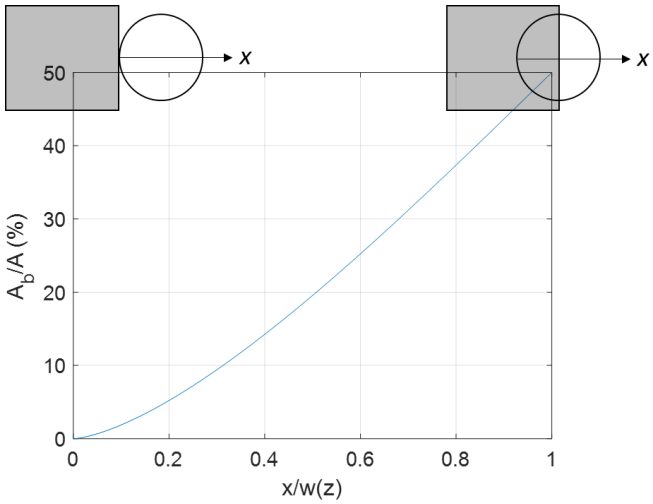

FIGURE 3. Variation of blocked area with knife-edge position.

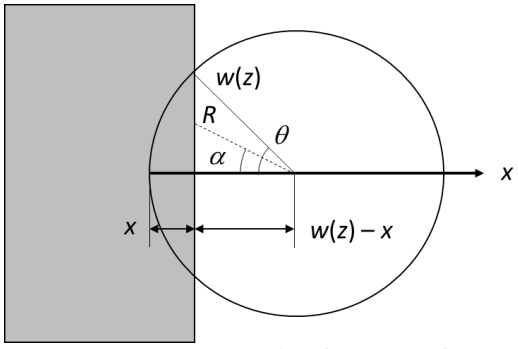

FIGURE 4. Geometry for incorporating radial intensity variation for beam cross-section.

The purely geometric model presented in Eq. 5 is not sufficient, however, because the beam intensity is not uniform across its cross-section, in general. Rather, it is often Gaussian and varies with the radial distance, r, from the beam axis, as described by Fig. 2 and Eq. 6, where I_0 is the maximum intensity at r = 0. If the knife-edge penetrates the beam at its waist (where z = 0), Eq. 6 simplifies to Eq. 7.

$$I(r,z) = I_0\left(\frac{w_0}{w(z)}\right)^2\exp\left(\frac{-2r^2}{w(z)^2}\right) \tag{6}$$

$$I(r) = I_0\exp\left(\frac{-2r^2}{{w_0}^2}\right) \tag{7}$$

To improve the geometric model, the cross-sectional intensity variation was incorporated.

Specifically, blocking the beam near its center (small r values) has a stronger effect on the photodetector output than blocking the beam far from its center. As shown in Fig. 4, however, the knife-edge does not block the beam at a single radius value. Rather, there is a continuous range of radii from ($w(z) - x$) along the x axis up to $w(z)$ as the angle θ is increased.

To proceed with the analysis, a mean radius value, R, may be calculated by integrating over the full θ range for each x value. The integration variable, α, is defined by Eq. 8. The mean radius is then calculated by rearranging Eq. 8 and writing the integral; see Eq. 9.

$$\alpha = \operatorname{acos}\left(\frac{w(z)-x}{R}\right) \tag{8}$$

$$R = \frac{1}{\theta}\int_0^{\theta} \frac{w(z)-x}{\cos\alpha}\, d\alpha = \frac{w(z)-x}{\theta}\int_0^{\theta} \sec\alpha\, d\alpha \tag{9}$$

Solving the Eq. 9 integral and evaluating over the integration limits gives Eq. 10, where θ is defined by Eq. 3, and the mean radius, R, depends on the knife-edge position, x. Both variables are normalized to the beam radius for plotting purposes.

$$R = \frac{w(z)-x}{\theta}\left(\ln|\sec\theta + \tan\theta| - \ln|\sec 0 + \tan 0|\right) \tag{10}$$

The next step is to substitute R for r in Eq. 6 to describe the intensity at the mean radius as a function of the knife-edge position. The final step is to multiply the Eq. 6 intensity factor by A_b from Eq. 5, where the effect is to "weight" the geometric solution by the exponential Gaussian intensity function. Example results for $w(z) = w_0$ are displayed in Fig. 5. For comparison purposes, the normalized blocked area curve from Fig. 4 is also included. It is observed that the slope is significantly affected. It is reduced near the beam edge, where the lower intensity portion of the beam cross-section is blocked, and increased near the center, where more of the higher intensity portion of the beam is blocked.

To complete the analysis, the Fig. 5 $(A_b/A)(I/I_0)$ result is scaled from 0 to 0.5 (i.e., the percent scaling is removed), mirrored about the vertical axis where $x/w(z) = 1$, and inverted to give the full available range of $x/w(z) = 0$ to 2 for the knife-edge position. Finally, this result is subtracted from 1 to mimic the normalized photodetector output, which is typically 1 when the beam is fully unblocked and 0 when the beam is fully blocked. See Fig. 6.

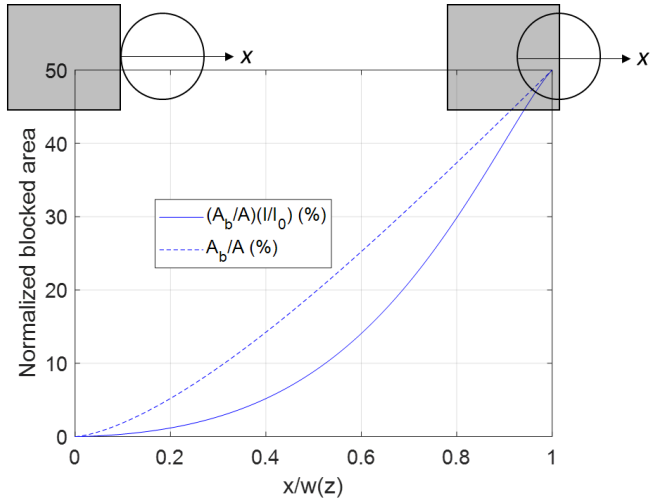

FIGURE 5. Normalized blocked area versus knife-edge position with (solid line) and without (dashed line) weighting by the normalized intensity at the mean beam radius for the knife-edge position.

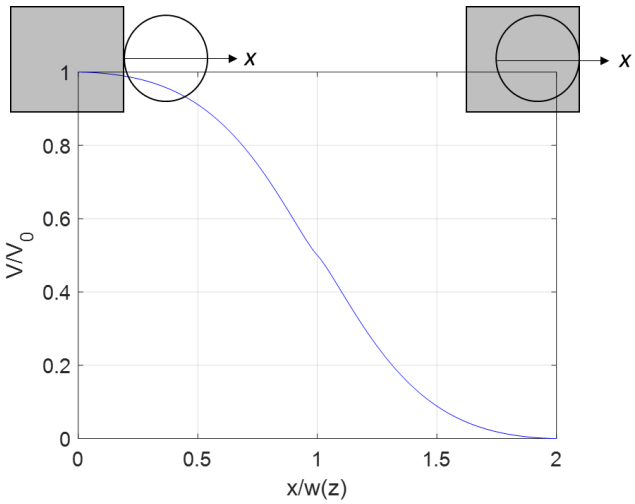

FIGURE 6. Modeled photodetector output displayed as normalized voltage versus normalized knife-edge position.

EXPERIMENTAL SETUP

To verify the model prediction, a photointerrupter (OMRON EE-SG3) was selected and a knife-edge (X-ACTO™ #17) was positioned within the beam using a linear air bearing stage (Aerotech ABL 10100-LT). The stage position was commanded and the photointerrupter output was measured, where the photointerrupter location was fixed and the knife-edge moved with the stage. The stage had a manufacturer-specified

positioning uncertainty of +/-0.2 µm and resolution of 0.5 nm. For the test sequence, the knife-edge was positioned outside the photointerrupter emitter-detector range and moved towards the sensor in 5 µm increments, with a 1 second dwell time, until the full range was exceeded (i.e., the beam was fully blocked).

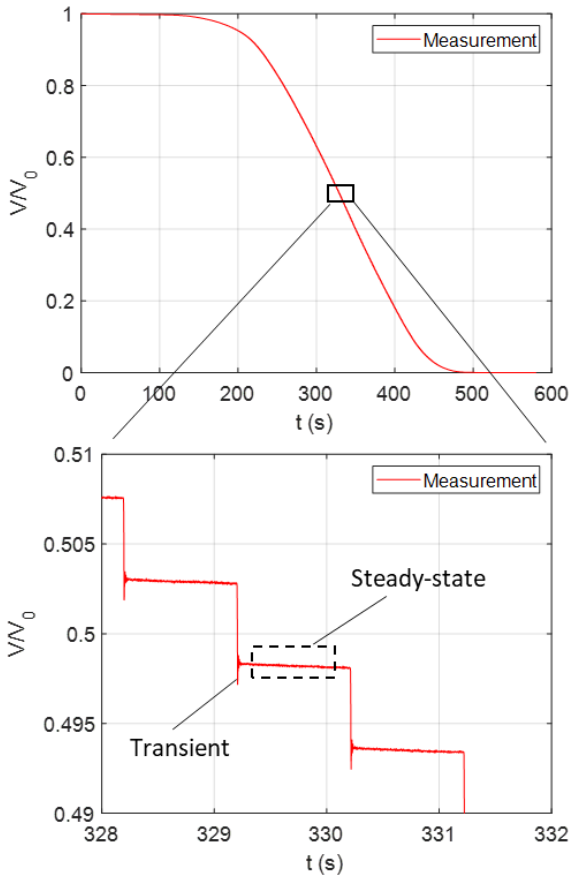

FIGURE 7. Time-domain normalized output voltage from the test sequence.

The total range of travel was approximately 2 mm and the corresponding working voltage was 2 V. The displacement-dependent output voltage was measured with a sampling frequency of 1000 Hz (Data Translation 9837B). A linear scaling technique was applied to the measured output voltage to normalize the voltage response. See Eq. 11, where V is the voltage for any knife-edge position, V_{min} is the fully blocked voltage and V_{max} is the fully unblocked voltage. The stepwise response for the test sequence is displayed in Fig. 7.

$$\frac{V}{V_0} = \frac{V - V_{min}}{V_{max} - V_{min}} \tag{11}$$

Next, the mean and standard deviation values for the steady-state portion of the stepwise response were determined. The steady-state response was selected to exclude the motion transient after each step; it was confirmed with a separate capacitance gage measurement that these transients were due to the stage control system and not the optical knife-edge displacement sensor. The result is presented in Fig. 8 with mean values and error bars that represent the type A measurement uncertainty (coverage factor of $k = 2$ on the calculated standard deviation) for the steady-state portion of each step.

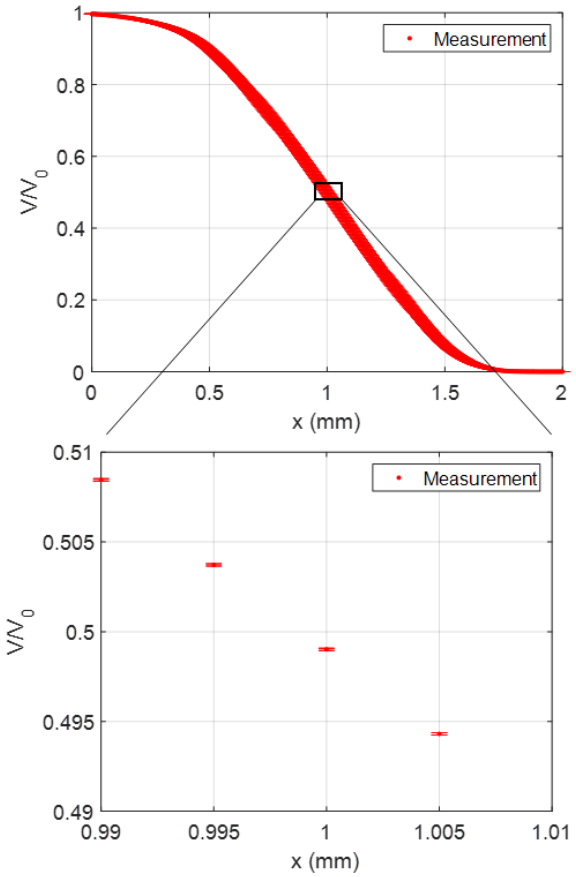

FIGURE 8. Stepwise optical knife-edge displacement sensor response with mean values and error bars, which identify standard deviations with a coverage factor of k = 2, for the normalized photointerrupter voltage.

RESULTS

The photodetector voltage output is compared to the model prediction in this section. Figure 9 displays the normalized voltage and model vs. knife-edge displacement, where it was assumed that the knife-edge penetrated the beam at its waist with a radius of 1 mm for the model. As

noted, no information was provided by the photointerrupter manufacturer regarding the waist location or beam radius, a 2 mm diameter hole was identified on the photointerrupter schematic as the laser source location. A 1 mm radius was therefore assumed with the waist located at the geometric center between the emitter and detector.

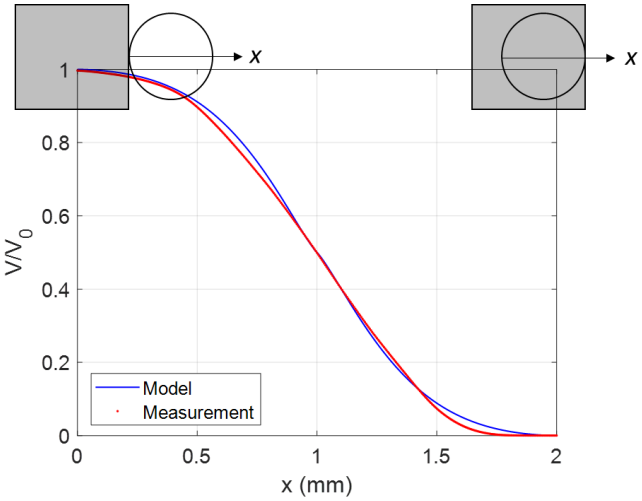

FIGURE 9. Comparison of measurement and model. The model assumed $w(z) = w_0 = 1$ mm in the absence of additional information from the photointerrupter manufacturer.

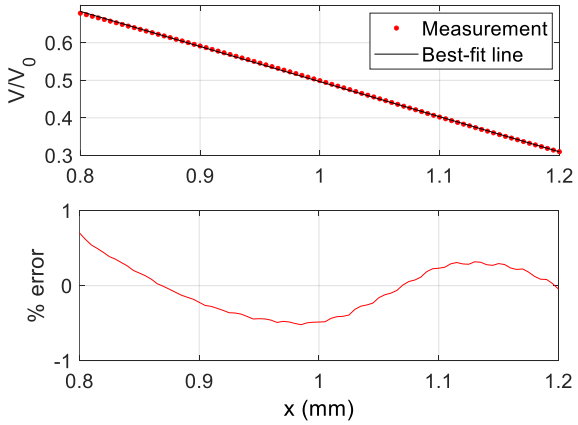

FIGURE 10. (Top) Linear section of measurement data with best-fit line. (Bottom) Percent error between the measurement data (normalized photointerrupter voltage) and best-fit line.

As noted, while the knife-edge position vs. photodetector voltage is nonlinear, it may be linearized by selecting the region where is the beam is approximately 50% blocked. For the model in Fig. 9, a range from 0.8 mm to 1.2 mm was chosen for analysis. The percent error between the normalized photodetector voltage and best-fit line is displayed in Fig. 10, where the slope of the best-fit line is -0. 9344 mm^{-1} with an R^2 value of 0.9998. It is observed that the error is less than 1% over the full range with some remaining structure. The corresponding percent error between the model and best-fit line over the same range is shown in Fig. 11, where the best-fit line slope is -0. 9991 mm^{-1} with an R^2 value of 0.9994. Again, the error is less than 1% with similar, but not identical, structure. The percent error between the modeled and measured slopes is 6.9%.

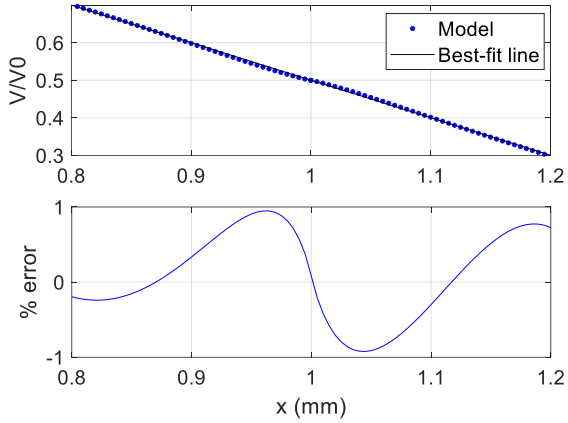

FIGURE 11. (Top) Linear section of model with best-fit line. (Bottom) Percent error between model and best-fit line.

CONCLUSIONS

This paper described the derivation and validation of an analytical model to predict the relationship between the knife-edge displacement and photointerrupter output for the well-known optical knife-edge displacement sensor. The model simultaneously considers the geometry of a rectangular knife-edge profile penetrating a circular laser beam perpendicular to the beam axis and the radially-symmetric Gaussian intensity profile for the beam cross-section.

Experiments were completed to compare the model to measured performance for a selected knife-edge and photodetector pair by prescribing known displacements using a linear air bearing stage. A stepwise pause-repeat positioning sequence was performed to compare the measured photointerrupter voltage to the model

prediction. It was found that the error between the predicted and measured slopes was 6.9% with errors less than 1% between the model/measurement and corresponding best-fit lines. Note that this agreement was obtained without calibration. The only input was the beam radius. The conclusion is that the model can be effectively applied as a design tool when implementing the optical knife-edge displacement sensor for measurement and control applications.

ACKNOWLEDGEMENTS

This manuscript has been authored by UT-Battelle, LLC, under contract DE-AC05-00OR22725 with the US Department of Energy (DOE). The US government retains and the publisher, by accepting the article for publication, acknowledges that the US government retains a nonexclusive, paid-up, irrevocable, worldwide license to publish or reproduce the published form of this manuscript, or allow others to do so, for US government purposes. DOE will provide public access to these results of federally sponsored research in accordance with the DOE Public Access Plan (http://energy.gov/downloads/doe-public-access-plan).

REFERENCES

1. Firester, A.H., Heller, M.E. and Sheng, P., 1977. Knife-edge scanning measurements of subwavelength focused light beams. Applied Optics, 16(7), pp.1971-1974.
2. de Araújo, M.A., Silva, R., de Lima, E., Pereira, D.P. and de Oliveira, P.C., 2009. Measurement of Gaussian laser beam radius using the knife-edge technique: Improvement on data analysis. Applied optics, 48(2), pp.393-396.
3. Karabacak, D., Kouh, T., Huang, C.C. and Ekinci, K.L., 2006. Optical knife-edge technique for nanomechanical displacement detection. Applied Physics Letters, 88(19), p.193122.
4. Chiu, Y. and Pan, J.H., 2007. Micro knife-edge optical measurement device in a silicon-on-insulator substrate. Optics Express, 15(10), pp.6367-6373.
5. Gu, G.M., Shin, Y.K., Son, J. and Kim, J., 2012. Design and characterization of a photo-sensor based force measurement unit (FMU). Sensors and Actuators A: Physical, 182, pp.49-56.
6. Gomez, M. and Schmitz, T., 2020. Low-cost, constrained-motion dynamometer for milling force measurement. Manufacturing Letters, 25, pp.34-39.
7. Gomez, M.F. and Schmitz, T.L., 2019. Displacement-based dynamometer for milling force measurement. Procedia Manufacturing, 34, pp.867-875.
8. Braunsmann, C., Prucker, V. and Schäffer, T.E., 2014. Optical knife-edge displacement sensor for high-speed atomic force microscopy. Applied Physics Letters, 104(10), p.103101.
9. Lee, C., Lee, S.K. and Tarbutton, J.A., 2014. Novel design and sensitivity analysis of displacement measurement system utilizing knife edge diffraction for nanopositioning stages. Review of Scientific Instruments, 85(9), p.095113.
10. Lee, C., Lee, S.K. and Tarbutton, J.A., 2015. Positioning control effectiveness of optical knife edge displacement sensor-embedded monolithic precision stage. Sensors and Actuators A: Physical, 233, pp.390-396.
11. Lee, C., Jeon, S., Stepanick, C.K., Zolfaghari, A. and Tarbutton, J.A., 2017. Investigation of optical knife edge sensor for low-cost, large-range and dual-axis nanopositioning stages. Measurement, 103, pp.157-164.
12. Zolfaghari, A., Jeon, S., Stepanick, C.K. and Lee, C., 2017. A novel sensor for two-degree-of-freedom motion measurement of linear nanopositioning stage using knife edge displacement sensing technique. Review of Scientific Instruments, 88(6), p.065110.
13. Kim, J.C., Kim, K.S. and Kim, S., 2013. Note: A compact three-axis optical force/torque sensor using photo-interrupters. Review of Scientific Instruments, 84(12), p.126109.
14. Lee, C., Mahajan, S.M., Zhao, R. and Jeon, S., 2016. A curved edge diffraction-utilized displacement sensor for spindle metrology. Review of Scientific Instruments, 87(7), p.075113.
15. Wang, C., Zhong, F. and Ellis, J.D., 2017. Two-dimensional straightness measurement based on optical knife-edge sensing. Review of Scientific Instruments, 88(9), p.095109.
16. Jeong, S., Chitalia, Y. and Desai, J.P., 2020. Miniature force sensor based on dual-photointerrupter with high linearity and disturbance compensation. IEEE Sensors Journal, 20(11), pp.5855-5864.
17. Lee, C., 2019. A first review of optical edge-diffraction technology for precision dimensional metrology. The International Journal of Advanced Manufacturing Technology, 102(5), pp.2465-2480.